

ALIGNING BRAIN FUNCTIONS BOOSTS THE DECODING OF VISUAL SEMANTICS IN NOVEL SUBJECTS

Alexis Thual*

Cognitive Neuroimaging Unit, INSERM, CEA, CNRS, NeuroSpin center, Gif sur Yvette, France
Mind, Inria Paris-Saclay, Palaiseau, France
alexis.thual@inria.fr

Yohann Benchetrit

FAIR, Meta
ybenchetrit@meta.com

Félix Geilert

FAIR, Meta
felixnext@meta.com

Jérémy Rapin

FAIR, Meta
jrapin@meta.com

Iurii Makarov

FAIR, Meta
iurii@meta.com

Hubert Banville

FAIR, Meta
hubertjb@meta.com

Jean-Rémi King

FAIR, Meta
Laboratoire des systèmes perceptifs, École normale supérieure
PSL University
jeanremi@meta.com

*Work done while interning at FAIR, Meta

ABSTRACT

Deep learning is leading to major advances in the realm of brain decoding from functional Magnetic Resonance Imaging (fMRI). However, the large inter-subject variability in brain characteristics has limited most studies to train models on one subject at a time. Consequently, this approach hampers the training of deep learning models, which typically requires very large datasets. Here, we propose to boost brain decoding by aligning brain responses to videos and static images across subjects. Compared to the anatomically-aligned baseline, our method improves out-of-subject decoding performance by up to 75%. Moreover, it also outperforms classical single-subject approaches when fewer than 100 minutes of data is available for the tested subject. Furthermore, we propose a new multi-subject alignment method, which obtains comparable results to that of classical single-subject approaches while improving out-of-subject generalization. Finally, we show that this method aligns neural representations in accordance with brain anatomy. Overall, this study lays the foundations for leveraging extensive neuroimaging datasets and enhancing the decoding of individuals with a limited amount of brain recordings.

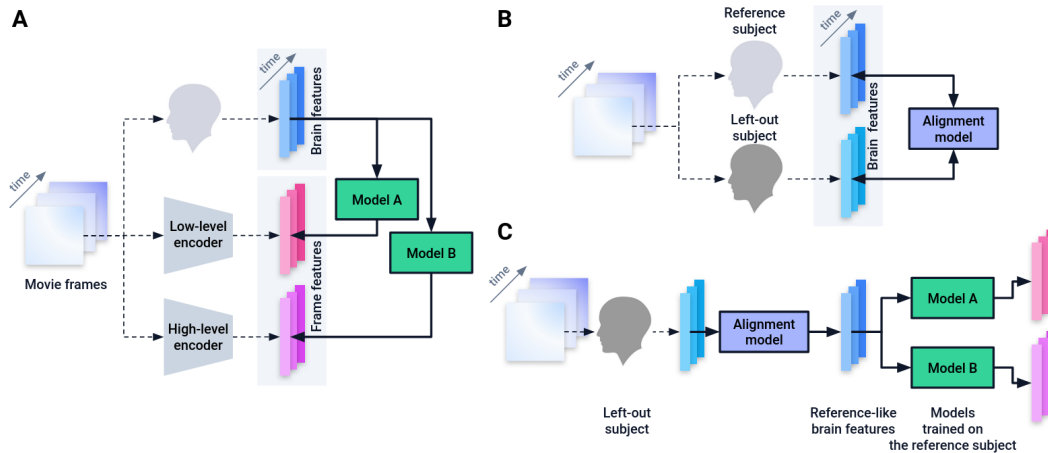


Figure 1: **General outline of video decoding from BOLD fMRI signal in left-out subjects**

A. For every image associated with a brain volume, one computes its low-level and high-level latent representations using pre-trained models. Subsequently, regression models can be fitted to map brain features onto each of these latent representations. **B.** BOLD signal acquired in two subjects watching the same movie can be used to derive an alignment model which associates voxels of the two subjects based on functional similarity. **C.** Once this alignment model is trained, it can be used to transform brain features of the left-out subject into brain features that resemble that of the reference subject. In particular, this allows one to use models that have been trained on a lot of data coming from a reference subject data, and apply it on a left-out subject for whom less data was collected.

1 INTRODUCTION

Decoding the brain Deep learning is greatly accelerating the possibility of decoding mental representations from brain activity. Originally restricted to linear models (Mitchell et al., 2004; Harrison & Tong, 2009; Haynes & Rees, 2006), the decoding of brain activity can now be carried out with deep learning techniques. In particular, using functional Magnetic Resonance Imaging (fMRI) signals, significant progress has been made in the decoding of images (Ozcelik & VanRullen, 2023; Chen et al., 2023a; Scotti et al., 2023; Takagi & Nishimoto, 2023; Gu et al., 2023; Ferrante et al., 2023; Mai & Zhang, 2023), speech (Tang et al., 2023), and videos (Kupersmidt et al., 2022; Wen et al., 2018; Wang et al., 2022; Chen et al., 2023b; Lahner et al., 2023; Phillips et al., 2022).

Challenge However, brain representations are highly variable across subjects, which makes it challenging to train a single model on multiple subjects using fMRI data. Therefore, with few noteworthy exceptions (Haxby et al., 2020; Ho et al., 2023), studies typically train a decoder on a single subject at a time. With this constraint in mind, major effort has been put towards building fMRI datasets collecting a lot of data in a limited number of participants (Allen et al., 2022; Wen et al., 2017; LeBel et al., 2023; Pinho et al., 2018). Nonetheless, the necessity to train and test models on a single subject constitutes a major impediment to using notoriously data-hungry deep learning approaches.

Functional alignment Several methods can align the functions – as opposed to the anatomy – of multiple brains, and thus offer a potential solution to inter-subject variability: differentiable wrappings of the cortical surface (Robinson et al., 2014), rotations between brain voxels in the functional space (Haxby et al., 2011), shared response models (Chen et al., 2015; Richard et al., 2020), permutations of voxels minimizing an optimal transport cost (Bazeille et al., 2019), or combinations of these approaches (Feilong et al., 2022). However, it is not clear which of these methods offers the best performance and generalization capabilities (Bazeille et al., 2021). Besides, several studies rely on deep learning models trained in a self-supervised fashion to obtain a useful embedding of brain activity, in hope that this embedding could be meaningful across subjects (Thomas et al., 2022; Chen et al., 2023a). However, it is currently unknown whether any of these methods improve the decoding of naturalistic stimuli such as videos, and how such hypothetical gain would vary with the amount of fMRI recording available in a given a subject.

Approach To address this issue, we leverage fMRI recordings of multiple subjects to boost the decoding of videos and static images in a single left-out subject. This requires fitting two models: an alignment model and a decoder. The alignment aims at making brain responses of a left-out subject most similar to those of a reference subject. Here, we leverage optimal transport to compute this transformation using functional and anatomical data from both subjects. The decoder consists of a linear regression trained to predict the latent representations of movie frames or static images from the corresponding BOLD signals or beta coefficients.

We evaluate video and image decoding in different setups. In particular, we assess (1) whether training a decoder with several subjects improves performance, (2) whether decoders generalize to subjects on which they were not trained and (3) the extent to which functional alignment improves aforementioned setups.

Contributions We first confirm the feasibility of decoding, from 3T fMRI, the semantics of videos watched by the subjects (Wen et al., 2017). We then confirm this approach with the decoding of static images from 7T fMRI (Allen et al., 2022). Our study further makes three novel contributions:

1. functional alignment across subjects boosts visual semantics decoding performance when left-out subjects have a limited amount of data
2. training a decoder on multiple aligned subjects reaches the same performance as training a single model per subject
3. the resulting alignments, computed from movie watching data, are anatomically coherent

2 METHODS

Our goal is to decode visual stimuli seen by subjects from their brain activity. To this end, we train a linear model to predict latent representations – shortened as *latents* – of these visual stimuli from BOLD fMRI signals recorded in subjects watching naturalistic videos.

In the considered data, brains are typically imaged at a rate of one scan every 2 seconds. During this period, a subject sees 60 video frames on average, or a static image for the case of Allen et al. (2022). For simplicity, we consider the restricted problem of decoding only the first video frame seen by subjects at each brain scan. Formally, regardless of the dataset, for a given subject, let $\mathbf{X} \in \mathbb{R}^{n,v}$ be the BOLD response collected in v voxels over n brain scans and $\mathbf{Y} \in \mathbb{R}^{n,m}$ the m -dimensional latent representation of each selected video frame for all n brain scans.

2.1 BRAIN ALIGNMENT

Anatomical alignment As a baseline, we consider the alignment method implemented in Freesurfer (Fischl, 2012), which relies on anatomical information to project each subject onto a surface template of the cortex (in our case *fsaverage5*). Consequently, brain data from all subjects lie on a mesh of size $v = 10\,242$ vertices per hemisphere.

Functional alignment On top of the aforementioned anatomical alignment, we apply a recent method from Thual et al. (2022) denoted as Fused Unbalanced Gromov-Wasserstein (FUGW) ¹. As illustrated in Figure 1.B, this method consists in using functional data to train an alignment that transforms brain responses of a given left-out subject into the brain responses of a reference subject. This approach can be seen as a soft permutation of voxels ² of the left-out subject which maximizes the functional similarity to voxels of the reference subject.

Formally, for a left-out subject, let $\mathbf{D}^{\text{out}} \in \mathbb{R}^{v,v}$ be the matrix of anatomical distances between vertices on the cortex, and $\mathbf{w}^{\text{out}} \in \mathbb{R}_+^v$ a probability distribution on vertices. \mathbf{w}^{out} can be interpreted as the relative importance of vertices ; without prior knowledge, we use the uniform distribution. Reciprocally, we define \mathbf{D}^{ref} and \mathbf{w}^{ref} for a reference subject. Note that, in the general case, v can be different from one subject to the other, although we simplify notations here.

We derive a transport plan $\mathbf{P} \in \mathbb{R}^{v,v}$ to match the vertices of the two subjects based on functional similarity, while preserving anatomical organisation. For this, we simultaneously optimize multiple constraints, formulated in the loss function $\mathcal{L}(\mathbf{P})$ described in Equation 1:

$$\mathcal{L}(\mathbf{P}) \triangleq (1 - \alpha) \underbrace{\sum_{0 \leq i,j < n} \|\mathbf{X}_i^{\text{out}} - \mathbf{X}_j^{\text{ref}}\|_2^2 \mathbf{P}_{i,j}}_{\text{Wasserstein loss}} + \alpha \underbrace{\sum_{0 \leq i,k,j,l < n} |\mathbf{D}_{i,k}^{\text{out}} - \mathbf{D}_{j,l}^{\text{ref}}|^2 \mathbf{P}_{i,j} \mathbf{P}_{k,l}}_{\text{Gromov-Wasserstein loss}} + \rho \left(\underbrace{\text{KL}(\mathbf{P}_{\#1} \otimes \mathbf{P}_{\#1} | \mathbf{w}^{\text{out}} \otimes \mathbf{w}^{\text{out}})}_{\text{Marginal constraints}} + \underbrace{\text{KL}(\mathbf{P}_{\#2} \otimes \mathbf{P}_{\#2} | \mathbf{w}^{\text{ref}} \otimes \mathbf{w}^{\text{ref}})}_{\text{Entropy}} \right) + \varepsilon \text{H}(\mathbf{P}) \quad (1)$$

with $\mathbf{P}_{\#1} \triangleq (\sum_j \mathbf{P}_{i,j})_{0 \leq i < v}$ and $\mathbf{P}_{\#2} \triangleq (\sum_i \mathbf{P}_{i,j})_{0 \leq j < v}$ the first and second marginal distributions of \mathbf{P} , \otimes the Kronecker product between two matrices, and $\text{KL}(\cdot, \cdot)$ the Kullback-Leibler divergence. α , ρ and ε are hyper-parameters setting the relative importance of each constraint.

Following Thual et al. (2022), we minimize $\mathcal{L}(\mathbf{P})$ with 10 iterations of a block coordinate descent algorithm (Séjourné et al., 2021), each running 1 000 Sinkhorn iterations (Cuturi, 2013). Subsequently, we define $\phi_{\text{out} \rightarrow \text{ref}}: \mathbf{X} \mapsto (\mathbf{P}^T \mathbf{X}^T) \oslash \mathbf{P}_{\#2} \in \mathbb{R}^{n,v}$ where \oslash is the element-wise division, a function which transports any matrix of brain features from the left-out subject to the reference subject. To simplify notations, for any \mathbf{X} defined on the left-out subject, we define $\mathbf{X}^{\text{out} \rightarrow \text{ref}} \triangleq \phi_{\text{out} \rightarrow \text{ref}}(\mathbf{X})$.

¹<https://alexisthual.github.io/fugw>

²We use the words *voxel* (volumetric pixel) or *vertex* (point on a mesh) indifferently.

2.2 DECODING

Brain input There is a time *lag* between the moment a stimulus is played and the moment it elicits a maximal BOLD response in the brain (Glover, 1999). Moreover, since the effect induced by this stimulus might span over multiple consecutive brain volumes, we set a *window size* describing the number of brain volumes to aggregate together. To account for these effects, we use a standard Finite Impulse Response (FIR) approach. FIR consists in fitting the decoder on a time-lagged, multi-volume version of the BOLD response. Different *aggregation functions* can be used, such as stacking or averaging. Figure S2 describes these concepts visually.

Video output The matrix of latent features \mathbf{Y} is obtained by using a pre-trained image encoder on each video frame and concatenating all obtained vectors in \mathbf{Y} . Similarly to Ozcelik & VanRullen (2023), and as illustrated in Figure 1.A, we seek to predict CLIP 257×768 (high-level) and VD-VAE (low-level) latent representations. We use visual – as opposed to textual – CLIP representations (Radford et al., 2021). For comparison, we also reproduce our approach on latent representations from CLIP CLS (high-level) and AutoKL (low-level), which happen to be much smaller³ and are computationally easier to fit.

Model Fitting the decoder consists in deriving $\mathbf{W} \in \mathbb{R}^{v,m}$, $\mathbf{b} \in \mathbb{R}^m$ the solution of a Ridge regression problem – i.e. a linear regression with L2 regularization – predicting \mathbf{Y} from \mathbf{X} .

Evaluation We evaluate the performance of the decoder with retrieval metrics. Let us denote \mathbf{X} and \mathbf{Y} the brain and latent features used to train the decoder, \mathbf{X}_{test} and \mathbf{Y}_{test} those to test the decoder, and $\hat{\mathbf{Y}} \triangleq \mathbf{W}\mathbf{X}_{\text{test}} + \mathbf{b}$ the predicted latents. We ensure that the train and test data are disjoint.

We randomly draw a retrieval set K of 499 frames without replacement from the test data. For each pair $\hat{\mathbf{y}}, \mathbf{y}$ of predicted and ground truth latents, one derives their cosine similarity score $s(\hat{\mathbf{y}}, \mathbf{y})$, as well as similarity scores to all latents \mathbf{y}_{neg} of the retrieval set $s(\hat{\mathbf{y}}, \mathbf{y}_{\text{neg}})$. Let us denote $r_K(\hat{\mathbf{y}}, \mathbf{y})$ the rank of \mathbf{y} , which we define as the number of elements of K whose similarity score to $\hat{\mathbf{y}}$ is larger than $s(\hat{\mathbf{y}}, \mathbf{y})$. In order for the rank to not depend on the size of K , we define the *relative rank* as $\frac{r(\hat{\mathbf{y}}, \mathbf{y})}{|K|}$. Finally, one derives the median relative rank $\text{MR}(\hat{\mathbf{Y}}, K)$:

$$r_K(\hat{\mathbf{y}}, \mathbf{y}) \triangleq |\{\mathbf{y}_{\text{neg}} \in K \mid s(\hat{\mathbf{y}}, \mathbf{y}_{\text{neg}}) > s(\hat{\mathbf{y}}, \mathbf{y})\}|$$

$$\text{MR}(\hat{\mathbf{Y}}, K) \triangleq \text{median}\left(\left\{\frac{r_K(\hat{\mathbf{y}}, \mathbf{y})}{|K|}, \forall (\hat{\mathbf{y}}, \mathbf{y})\right\}\right)$$

2.3 DECODING AND ALIGNMENT SETUPS

Within- vs out-of-subject The *within-subject* setup consists in training a decoder with data $\mathbf{X}_{\text{train}}^{S_1}, \mathbf{Y}_{\text{train}}^{S_1}$ from a given subject, and testing it on left-out data $\mathbf{X}_{\text{test}}^{S_1}, \mathbf{Y}_{\text{test}}^{S_1}$ acquired in the same subject. The *out-of-subject* setup consists in training a decoder with data from a given subject, and testing it on data $\mathbf{X}_{\text{test}}^{S_2}, \mathbf{Y}_{\text{test}}^{S_2}$ acquired in a left-out subject.

Single- vs multi-subject The *single-subject* setup consists in training a decoder predicting \mathbf{Y} from \mathbf{X} for each subject. The *multi-subject* setup consists in training a single decoder using data from multiple subjects. In this case, data from several subjects is stacked together, resulting in a matrix $\mathbf{X}_{\text{multi}} \in \mathbb{R}^{n_1 + \dots + n_p, v}$ and $\mathbf{Y}_{\text{multi}} \in \mathbb{R}^{n_1 + \dots + n_p, m}$, where p is the number of subjects.

Un-aligned vs aligned In multi-subject and out-of-subject setups, data coming from different subjects can be *functionally aligned* to that of a *reference* subject. Let us assume that S_1 is the reference subject. In the case of multi-subject, all subjects are aligned to S_1 and the decoder is trained on a concatenation of $\mathbf{X}^{S_1}, \mathbf{X}^{S_2 \rightarrow S_1}, \dots, \mathbf{X}^{S_p \rightarrow S_1}$ (see notations introduced at the end of section 2.1) and $\mathbf{Y}^{S_1}, \dots, \mathbf{Y}^{S_p}$, where p is the number of subjects. In the case of out-of-subject, it corresponds to aligning S_2 onto S_1 , such that a decoder trained on S_1 will be tested on $\mathbf{X}_{\text{test}}^{S_2 \rightarrow S_1}, \mathbf{Y}_{\text{test}}^{S_2}$.

The aforementioned setups are described visually in Figure 3.A.

³Dimensions for CLIP CLS: 768 ; CLIP 257×768 : $257 \times 768 = 197\,376$; AutoKL: $4 \times 32 \times 32 = 4\,096$; VD-VAE: $2 \times 2^4 + 4 \times 2^8 + 8 \times 2^{10} + 16 \times 2^{12} + 2^{14} = 91\,168$

Evaluation under different data regimes Note that alignment and decoding models need not be fitted using the same amount of data. In particular, we are interested in evaluating out-of-subject performance in setups where a lot of data is available for a *reference* subject, and little data is available for a *left-out* subject: this would typically be the case in clinical setups where little data is available in patients. In this case, we evaluate whether it is possible to use this small amount of data to align the left-out subject onto the reference subject, and have the left-out subject benefit from a decoder previously trained on a lot of data.

2.4 DATASETS

We analyze two fMRI datasets. The first dataset (Wen et al., 2017) comprises 3 human subjects who each watched 688 minutes of video. The videos consists of 18 train segments of 8 minutes each and 5 test segments of 8 minutes each. Each training segment was presented twice. Each test segment was presented 10 times. Each segment consists of a sequence of roughly 10-second video clips. The fMRI data was acquired at 3 Tesla (3T), 3.5mm isotropic spatial resolution and 2-second temporal resolution. It was minimally pre-processed with the same pre-processing pipeline than that of the Human Connectome Project (Glasser et al., 2013). In particular, data from each subject are projected onto a common volumetric anatomical template. Similarly to prior work on this dataset (Wen et al., 2018; Kupersmidt et al., 2022; Wang et al., 2022), we use runs related to the first 18 video segments - 288 minutes - as training data, and runs related to the last 5 video segments as test data.

The second dataset (Allen et al., 2021) comprises 8 subjects who are shown 10 000 static images three times. They were scanned over 40 sessions of 60 minutes, amounting to 2 400 minutes of data. Instead of raw BOLD signal, we leverage precomputed beta coefficients accessible online. Supplementary section A.4 describes this dataset in more detail.

2.5 PREPROCESSING

For the Wen et al. (2017) dataset, we implement minimal additional preprocessing steps for each subject separately. For this, we (1) project all volumetric data onto the FreeSurfer average surface template *fsaverage5* (Fischl, 2012), then (2) regress out cosine drifts in each vertex and each run and finally (3) center and scale each vertex time-course in each run. Figure S1 gives a visual explanation as to why the last two steps are needed. The first two steps are implemented with *nilearn* (Abraham et al., 2014)⁴ and the last one with *scikit-learn* (Pedregosa et al., 2011).

Additionally, for a given subject, we try out two different setups: a first one where runs showing the same video are averaged, and a second one where they are stacked.

The Allen et al. (2021) dataset is already preprocessed by the original authors, and maps of beta coefficients are accessible online.

2.6 HYPER-PARAMETERS SELECTION

To train decoders, we use the same regularization coefficient α_{ridge} across latent types and choose it by running a cross-validated grid search on folds of the training data. We find that results are robust to using different values and therefore set $\alpha_{\text{ridge}} = 50\,000$. Similarly, values for lag, window size and aggregation function are determined through a cross-validated grid search.

Finally, for functional alignment, we use default parameters shipped with version 0.1.0 of FUGW. Namely, α , which controls the balance between Wasserstein and Gromov-Wasserstein losses – i.e. how important functional data is compared to anatomical data – is set to 0.5. Empirically, we see that $\alpha = 0.5$ yields values for the Wasserstein loss which are bigger than that of the Gromov-Wasserstein loss, meaning that functional data drives these alignments. ε , which controls for entropic regularization – i.e. how blurry computed alignments will be – is set to 10^{-4} . Empirically, this value yields alignments which are anatomically very sharp. ρ , which sets the importance of marginal constraints – i.e. to what extent more or less mass can be transported to / from each voxel – is set to 1. Empirically, this value leads to all voxels being transported / matched.

⁴<https://nilearn.github.io>

3.2 OUT-OF-SUBJECT DECODING AND MULTI-SUBJECT TRAINING

Main results As illustrated in Figure 3, models trained on one subject do not generalise well to other subjects. However, we demonstrate that functional alignment can successfully be used as a transfer learning strategy to generalize a pre-trained model to left-out subjects. In particular, we show that left-out subjects need not have the same amount of available data than training subjects to benefit from their model: with just 30 minutes of data, left-out subjects can reach performance which would have needed roughly 100 minutes of data in a within-subject setting. Besides, compared to the out-of-subject baseline, we obtain 25 to 75 percents improvement in relative median rank across latent types.

Besides, we show that a single model trained on all functionally aligned subjects can reach slightly better results than models trained on all un-aligned subjects. In every subject, this multi-subject aligned model performs comparably to their associated within-subject model.

Note that, in Figure 3, we chose the best performing subject (S2) as the reference subject. We report all other combinations of reference and left-out subjects in Supplementary Figures S6 and S7 and find that all effects persist regardless of the combination. Moreover, supplementary Figures S8 and S9 show that these results hold for all types for latents. Furthermore, we replicate this experiment on four subjects from the Natural Scenes Dataset (Allen et al., 2022). The results, based on the decoding of static images, are similar to those obtained for video decoding (Tables S1 and S2).

Finally, Figures S11, S12, S13, S14 present all other setups we ran for this study. In particular, they show that a multi-subject aligned model (e.g. trained on S1 and S2) has better performance on aligned left-out subjects (e.g. S3) than a single-subject model (e.g. trained on S2 only).

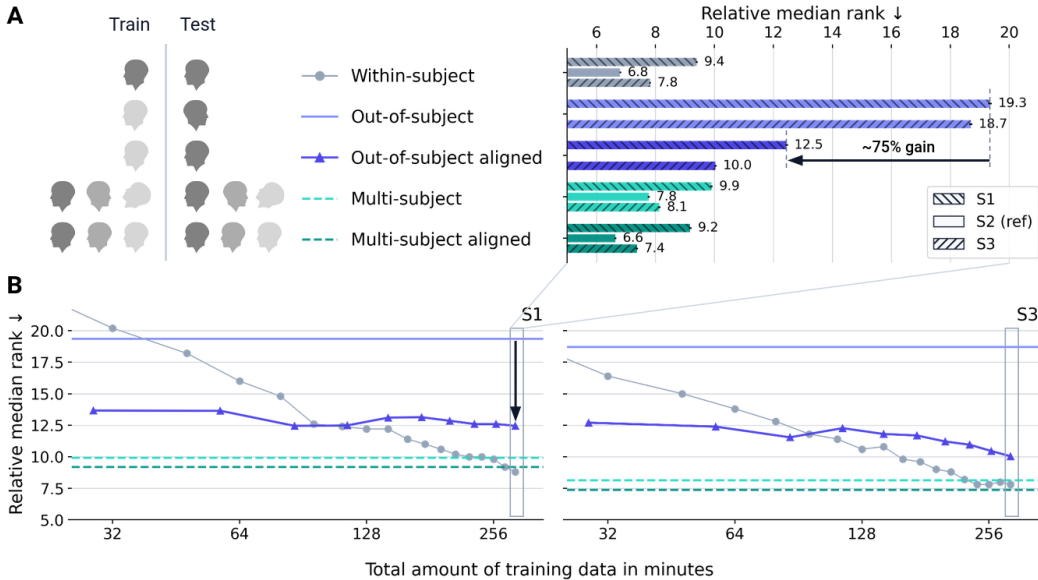


Figure 3: Effects of functional alignment on multi-subject and out-of-subject setups
 We report relative median rank \downarrow in all setups described in section 2.3 for CLIP 257 \times 768. In all *aligned* cases, S1 and S3 were aligned onto S2. In all *out-of-subject* cases, we test S1 and S3 onto a decoder trained on S2. In all *multi-subject* cases, the decoder was trained on all data from all 3 subjects. **A.** In this panel, all models (alignment and decoding) were trained on all available training data. Results for other latent types are available in Figure S8. **B.** In left-out S1 and S3, decoding performance is much better when using functional alignment to S2 (solid dark purple) than when using anatomical alignment only (solid pale purple). Performance increases slightly as the amount of data used to align subjects grows, but does not always reach levels which can be achieved with a single-subject model fitted in left-out subjects (solid pale gray dots) when a lot of training data is available. Training a model on multiple subjects yields good performance in all 3 subjects (dashed pale teal) which can be further improved by using functional alignment (dashed dark teal). Results for other latent types are available in Figure S9.

Exploring computed alignments To better understand how brain features are transformed by functional alignment, we show in Figure 4 how vertices from S1 are permuted to fit those of S2. Note that both subjects’ data lie on fsaverage5. To this end, we colorize vertices in S1 using the MMP 1.0 atlas (Glasser et al., 2016) and use $\phi_{S1 \rightarrow S2}$ to transport each of the three RGB channels of this colorization. We see that, even in low data regimes, FUGW scrambles most of the brain but can leverage signal to recover the cortical organization of the occipital lobe. Higher regimes yield anatomically-consistent matches in a much higher number of cortical areas such as the temporal and parietal lobes, and more surprisingly in the primary motor cortex as well, while the prefrontal cortex and temporo-parietal junction (TPJ) still seem challenging to map.

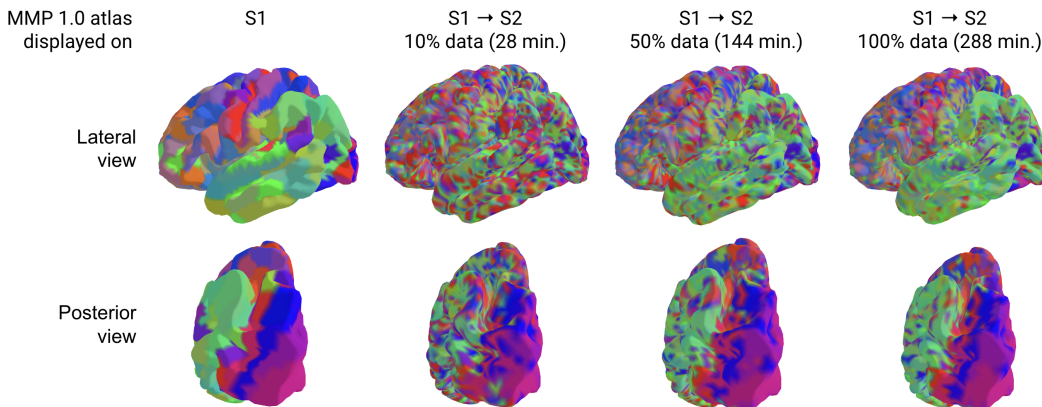


Figure 4: **Visualizing functional alignments in the left hemisphere** Vertices of the left-out subject (left) are permuted by FUGW. The result of this permutation is visualized on the reference subject (columns 2, 3, and 4). Fitting FUGW with different increasing amounts of data gradually unfolds the cortical organisation of multiple areas, even non-visual ones. Note that all 3 models have been fitted using the same number of iterations.

3.3 INFLUENCE OF TRAINING SET SIZE AND TEST SET REPETITIONS

Recent publications in brain-decoding using non-invasive brain imagery show impressive results. However, we stress that these results are obtained in setups which are very advantageous when it comes to both dataset size and signal-to-noise ratio. To better assess the importance of these two factors, we report in Figure 5 performance metrics for subject models trained and tested with various amounts of data and various amounts of noise.

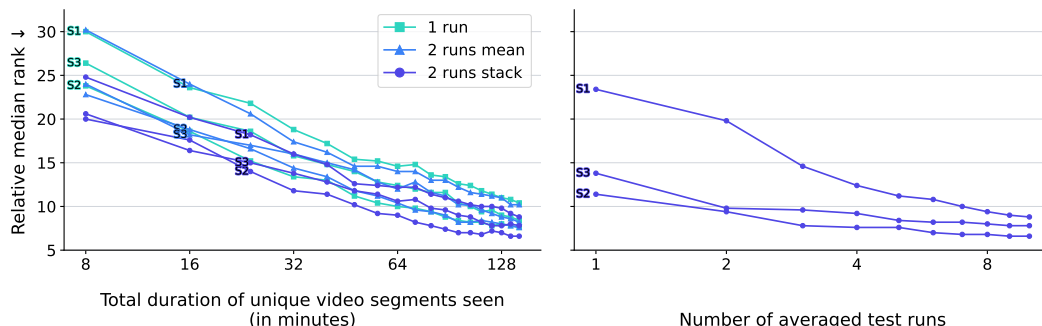


Figure 5: **Effect of training set size and test set noise on retrieval metrics** Relative median rank \downarrow on a fixed test set gets better as more training data is used to fit the model (left). Interestingly, averaging brain volumes of 2 similar runs does not bring improvements compared to using just 1 run. Instead, stacking runs does yield significant improvements. Note that training sets using 2 runs have twice as much data as those affected using 1 run. Finally, these metrics are highly affected by the noise level of the test set (right): averaging more runs in the test set yields better metrics despite using the same decoder.

Firstly, using a fixed test set in which brain features were averaged across runs, we find that exponentially more training data is required per subject to achieve better performance. This finding is similar to that of systematic scaling studies on similar topics (Tang et al., 2023). More interestingly, in this given signal-to-noise ratio setup, it seems that more diverse training data should bring comparable or better performance than repeating already seen content, while potentially covering more semantic domains.

Secondly, reported performance metrics only hold in favorable signal-to-noise setups. Indeed, the test set associated with the Wen 2017 dataset comes with 10 runs for each video segment, which, when averaged together, greatly reduce the noise level. However, as reported here, when tested in real-life signal-to-noise conditions (i.e. only one run per video clip), our models’ performance degrades: it is approximately twice as bad for each subject when using CLIP latents.

4 DISCUSSION

Impact The present work confirms the feasibility of using fMRI signals in response to natural images and videos to decode high level visual features (Nishimoto et al., 2011). It further demonstrates that it is possible to leverage these fMRI signals to estimate meaningful functional alignments between subjects, and use them to transfer semantic decoders to novel subjects.

In particular, our study shows that decoding brain data from a left-out subject can be substantially improved by aligning this left-out subject to a large reference dataset on which a decoder was trained. Our method thus paves the way towards using models trained on large amounts of individual data to decode signal acquired in smaller neuroimaging studies, which typically record one hour of fMRI for each subject (Madan, 2022).

Besides, this study reports decoding accuracy in setups where subjects are showed test stimuli for the first time only, hence yielding insights on how these models would perform in real-time decoding. While performance improves with the number of repetitions at test time, reasonable decoding performance of semantics can be achieved in two out of three subjects with just one repetition.

Lastly, by systematically quantifying decoding accuracy as a function of the amount of training data, the present work brings insightful recommendations as to what stimuli should be played in future fMRI datasets collecting large amounts of data in a limited number of subjects. In the current setup (naturalistic movies acquired at 3T), more diverse semantic content is more valuable than repeated content for fitting decoding models.

Limitations This work is a first step towards training accurate semantic decoders which generalize across individuals, but subsequent work remains necessary to ensure the generality of our findings.

Firstly, although reported gains in out-of-subject setups are significant, the small number of participants present in the dataset under study calls for replications on other – and potentially larger – cohorts. However, to our knowledge, no other dataset presented similar features to that of Wen et al. (2017) – i.e. high quantity of data per subject and large variety of video stimuli.

Secondly, our approach currently requires left-out subjects to watch the same videos as reference subjects. It is yet unclear whether functional alignment could bring improvements without this constraint. However, multi-subject decoding can probably help partially address this issue: since it is possible to train a decoder on multiple subjects and because not all of them have to watch the same movies, it is possible that a lot of different movies could be used as “anchors” for left-out individuals.

Thirdly, our method relies on pre-trained encoders, and cannot align all subjects at once. Consequently, overall performance highly depends on the quality of other models and of data acquired in reference individuals. Recent work in perception decoding in MEG shows that these two constraints might be alleviated (Défossez et al., 2022; Benchetrit et al., 2023), although it is not sure the underlying methods would work on fMRI data.

Finally, while restricting this study to linear models makes sense to establish baselines and ensure replicability, non-linear models have proved to be as least comparably efficient (Scotti et al., 2023). A natural improvement on this work could include these architectures.

Ethical implications Out-of-subject generalization is an important test for decoding models, but it raises legitimate concerns. In this regard, this study highlights that signal-to-noise ratio still currently makes it challenging to very accurately decode semantics in a real-time setup, and that a non-trivial amount of data is needed per individual for these models to work. Moreover, we stress that, while great progress has been made in decoding perceived stimuli, imagined stimuli are still very challenging to decode (Horikawa & Kamitani, 2017). Nonetheless, it is important for advances in this domain to be publicly documented. We thus advocate that open and peer-reviewed research is the best way forward to safely explore the implications of inter-subject modeling, and more generally brain decoding.

Conclusion Overall, these results provide a significant step towards real-time, subject-agnostic visual decoding of semantics using fMRI.

ACKNOWLEDGEMENTS

This work was funded in part by FrontCog grant ANR-17-EURE-0017 to JRK for his work at PSL. We would like to thank Bertrand Thirion, Stanislas Dehaene and Pierre Orhan for their valuable comments.

REFERENCES

- Alexandre Abraham, Fabian Pedregosa, Michael Eickenberg, Philippe Gervais, Andreas Mueller, Jean Kossaifi, Alexandre Gramfort, Bertrand Thirion, and Gael Varoquaux. Machine learning for neuroimaging with scikit-learn. *Frontiers in Neuroinformatics*, 8, 2014. ISSN 1662-5196. URL <https://www.frontiersin.org/article/10.3389/fninf.2014.00014>.
- Emily J. Allen, Ghislain St-Yves, Yihan Wu, Jesse L. Breedlove, Jacob S. Prince, Logan T. Dowlle, Matthias Nau, Brad Caron, Franco Pestilli, Ian Charest, J. Benjamin Hutchinson, Thomas Naselaris, and Kendrick Kay. A massive 7T fMRI dataset to bridge cognitive neuroscience and artificial intelligence. *Nature Neuroscience*, pp. 1–11, December 2021. ISSN 1546-1726. doi: 10.1038/s41593-021-00962-x. URL <https://www.nature.com/articles/s41593-021-00962-x>. Bandiera_abtest: a Cg_type: Nature Research Journals Primary_atype: Research Publisher: Nature Publishing Group Subject.term: Cortex;Neural encoding;Object vision;Perception Subject.term.id: cortex;neural-encoding;object-vision;perception.
- Emily J. Allen, Ghislain St-Yves, Yihan Wu, Jesse L. Breedlove, Jacob S. Prince, Logan T. Dowlle, Matthias Nau, Brad Caron, Franco Pestilli, Ian Charest, J. Benjamin Hutchinson, Thomas Naselaris, and Kendrick Kay. A massive 7T fMRI dataset to bridge cognitive neuroscience and artificial intelligence. *Nature Neuroscience*, 25(1):116–126, January 2022. ISSN 1546-1726. doi: 10.1038/s41593-021-00962-x. URL <https://www.nature.com/articles/s41593-021-00962-x>. Number: 1 Publisher: Nature Publishing Group.
- T. Bazeille, H. Richard, H. Janati, and B. Thirion. Local Optimal Transport for Functional Brain Template Estimation. In Albert C. S. Chung, James C. Gee, Paul A. Yushkevich, and Siqi Bao (eds.), *Information Processing in Medical Imaging*, Lecture Notes in Computer Science, pp. 237–248, Cham, 2019. Springer International Publishing. ISBN 978-3-030-20351-1. doi: 10.1007/978-3-030-20351-1_18.
- Thomas Bazeille, Elizabeth DuPre, Hugo Richard, Jean-Baptiste Poline, and Bertrand Thirion. An empirical evaluation of functional alignment using inter-subject decoding. *NeuroImage*, 245:118683, December 2021. ISSN 1053-8119. doi: 10.1016/j.neuroimage.2021.118683. URL <https://www.sciencedirect.com/science/article/pii/S1053811921009563>.
- Yohann Benchetrit, Hubert Banville, and Jean-Rémi King. Brain decoding: toward real-time reconstruction of visual perception. *arXiv preprint arXiv:2310.19812*, 2023.
- Po-Hsuan (Cameron) Chen, Janice Chen, Yaara Yeshurun, Uri Hasson, James Haxby, and Peter J Ramadge. A Reduced-Dimension fMRI Shared Response Model. In *Advances in Neural Information Processing Systems*, volume 28. Curran Associates, Inc., 2015. URL https://papers.nips.cc/paper_files/paper/2015/hash/b3967a0e938dc2a6340e258630febd5a-Abstract.html.
- Zijiao Chen, Jiaxin Qing, Tiange Xiang, Wan Lin Yue, and Juan Helen Zhou. Seeing Beyond the Brain: Conditional Diffusion Model with Sparse Masked Modeling for Vision Decoding, March 2023a. URL <http://arxiv.org/abs/2211.06956>. arXiv:2211.06956 [cs].
- Zijiao Chen, Jiaxin Qing, and Juan Helen Zhou. Cinematic Mindscapes: High-quality Video Reconstruction from Brain Activity, May 2023b. URL <http://arxiv.org/abs/2305.11675>. arXiv:2305.11675 [cs].
- Marco Cuturi. Sinkhorn Distances: Lightspeed Computation of Optimal Transportation Distances. *arXiv*, June 2013. doi: 10.48550/arXiv.1306.0895.
- Alexandre Défossez, Charlotte Caucheteux, Jérémy Rapin, Ori Kabeli, and Jean-Rémi King. Decoding speech from non-invasive brain recordings, August 2022. URL <http://arxiv.org/abs/2208.12266>. arXiv:2208.12266 [cs, eess, q-bio].
- Ma Feilong, Samuel A. Nastase, Guo Jiahui, Yaroslav O. Halchenko, M. Ida Gobbini, and James V. Haxby. The Individualized Neural Tuning Model: Precise and generalizable cartography of functional architecture in individual brains, May 2022. URL <https://www.biorxiv.org/content/10.1101/2022.05.15.492022v1>. Pages: 2022.05.15.492022 Section: New Results.

- Matteo Ferrante, Furkan Ozcelik, Tommaso Boccato, Rufin VanRullen, and Nicola Toschi. Brain Captioning: Decoding human brain activity into images and text, May 2023. URL <http://arxiv.org/abs/2305.11560>. arXiv:2305.11560 [cs].
- Bruce Fischl. FreeSurfer. *NeuroImage*, 62(2):774–781, August 2012. ISSN 1053-8119. doi: 10.1016/j.neuroimage.2012.01.021. URL <https://www.sciencedirect.com/science/article/pii/S1053811912000389>.
- Matthew F. Glasser, Stamatiou N. Sotiropoulos, J. Anthony Wilson, Timothy S. Coalson, Bruce Fischl, Jesper L. Andersson, Junqian Xu, Saad Jbabdi, Matthew Webster, Jonathan R. Polimeni, David C. Van Essen, Mark Jenkinson, and WU-Minn HCP Consortium. The minimal preprocessing pipelines for the Human Connectome Project. *NeuroImage*, 80:105–124, October 2013. ISSN 1095-9572. doi: 10.1016/j.neuroimage.2013.04.127.
- Matthew F. Glasser, Timothy S. Coalson, Emma C. Robinson, Carl D. Hacker, John Harwell, Essa Yacoub, Kamil Ugurbil, Jesper Andersson, Christian F. Beckmann, Mark Jenkinson, Stephen M. Smith, and David C. Van Essen. A multi-modal parcellation of human cerebral cortex. *Nature*, 536(7615):171–178, August 2016. ISSN 1476-4687. doi: 10.1038/nature18933. URL <https://www.nature.com/articles/nature18933>. Number: 7615 Publisher: Nature Publishing Group.
- G. H. Glover. Deconvolution of impulse response in event-related BOLD fMRI. *NeuroImage*, 9(4): 416–429, April 1999. ISSN 1053-8119. doi: 10.1006/nimg.1998.0419.
- Zijin Gu, Keith Jamison, Amy Kuceyeski, and Mert Sabuncu. Decoding natural image stimuli from fMRI data with a surface-based convolutional network, March 2023. URL <http://arxiv.org/abs/2212.02409>. arXiv:2212.02409 [cs, q-bio].
- Stephanie A Harrison and Frank Tong. Decoding reveals the contents of visual working memory in early visual areas. *Nature*, 458(7238):632–635, 2009.
- James V. Haxby, J. Swaroop Guntupalli, Andrew C. Connolly, Yaroslav O. Halchenko, Bryan R. Conroy, M. Ida Gobbini, Michael Hanke, and Peter J. Ramadge. A common, high-dimensional model of the representational space in human ventral temporal cortex. *Neuron*, 72(2):404–416, October 2011. ISSN 1097-4199. doi: 10.1016/j.neuron.2011.08.026.
- James V Haxby, J Swaroop Guntupalli, Samuel A Nastase, and Ma Feilong. Hyperalignment: Modeling shared information encoded in idiosyncratic cortical topographies. *eLife*, 9:e56601, June 2020. ISSN 2050-084X. doi: 10.7554/eLife.56601. URL <https://doi.org/10.7554/eLife.56601>. Publisher: eLife Sciences Publications, Ltd.
- John-Dylan Haynes and Geraint Rees. Decoding mental states from brain activity in humans. *Nature reviews neuroscience*, 7(7):523–534, 2006.
- Jun Kai Ho, Tomoyasu Horikawa, Kei Majima, Fan Cheng, and Yukiyasu Kamitani. Inter-individual deep image reconstruction via hierarchical neural code conversion. *NeuroImage*, 271:120007, May 2023. ISSN 1053-8119. doi: 10.1016/j.neuroimage.2023.120007. URL <https://www.sciencedirect.com/science/article/pii/S1053811923001532>.
- Tomoyasu Horikawa and Yukiyasu Kamitani. Generic decoding of seen and imagined objects using hierarchical visual features. *Nat. Commun.*, 8(15037):1–15, May 2017. ISSN 2041-1723. doi: 10.1038/ncomms15037.
- Ganit Kupersmidt, Roman Belyi, Guy Gaziv, and Michal Irani. A Penny for Your (visual) Thoughts: Self-Supervised Reconstruction of Natural Movies from Brain Activity, June 2022. URL <http://arxiv.org/abs/2206.03544>. arXiv:2206.03544 [cs].
- Benjamin Lahner, Kshitij Dwivedi, Polina Iamshchinina, Monika Graumann, Alex Lascelles, Gemma Roig, Alessandro Thomas Gifford, Bowen Pan, SouYoung Jin, N. Apurva Ratan Murty, Kendrick Kay, Aude Oliva, and Radoslaw Cichy. BOLD Moments: modeling short visual events through a video fMRI dataset and metadata, March 2023. URL <https://www.biorxiv.org/content/10.1101/2023.03.12.530887v1>. Pages: 2023.03.12.530887 Section: New Results.

- Amanda LeBel, Lauren Wagner, Shailee Jain, Aneesh Adhikari-Desai, Bhavin Gupta, Allyson Morgenthal, Jerry Tang, Lixiang Xu, and Alexander G. Huth. A natural language fMRI dataset for voxelwise encoding models. *Scientific Data*, 10(1):555, August 2023. ISSN 2052-4463. doi: 10.1038/s41597-023-02437-z. URL <https://www.nature.com/articles/s41597-023-02437-z>. Number: 1 Publisher: Nature Publishing Group.
- Christopher R. Madan. Scan Once, Analyse Many: Using Large Open-Access Neuroimaging Datasets to Understand the Brain. *Neuroinformatics*, 20(1):109–137, January 2022. ISSN 1559-0089. doi: 10.1007/s12021-021-09519-6.
- Weijian Mai and Zhijun Zhang. UniBrain: Unify Image Reconstruction and Captioning All in One Diffusion Model from Human Brain Activity, August 2023. URL <http://arxiv.org/abs/2308.07428>. arXiv:2308.07428 [cs].
- Tom M Mitchell, Rebecca Hutchinson, Radu S Niculescu, Francisco Pereira, Xuerui Wang, Marcel Just, and Sharlene Newman. Learning to decode cognitive states from brain images. *Machine learning*, 57:145–175, 2004.
- Shinji Nishimoto, An T. Vu, Thomas Naselaris, Yuval Benjamini, Bin Yu, and Jack L. Gallant. Reconstructing visual experiences from brain activity evoked by natural movies. *Current Biology*, 21(19):1641–1646, October 2011. ISSN 0960-9822. doi: 10.1016/j.cub.2011.08.031. URL <https://www.ncbi.nlm.nih.gov/pmc/articles/PMC3326357/>.
- Furkan Ozelik and Rufin VanRullen. Natural scene reconstruction from fMRI signals using generative latent diffusion, June 2023. URL <http://arxiv.org/abs/2303.05334>. arXiv:2303.05334 [cs, q-bio].
- Fabian Pedregosa, Gaël Varoquaux, Alexandre Gramfort, Vincent Michel, Bertrand Thirion, Olivier Grisel, Mathieu Blondel, Peter Prettenhofer, Ron Weiss, Vincent Dubourg, Jake Vanderplas, Alexandre Passos, David Cournapeau, Matthieu Brucher, Matthieu Perrot, and Édouard Duchesnay. Scikit-learn: Machine Learning in Python. *Journal of Machine Learning Research*, 12(85):2825–2830, 2011. ISSN 1533-7928. URL <http://jmlr.org/papers/v12/pedregosa11a.html>.
- Erin M. Phillips, Kirsten D. Gillette, Daniel D. Dilks, and Gregory S. Berns. Through a Dog’s Eyes: fMRI Decoding of Naturalistic Videos from the Dog Cortex. *JoVE (Journal of Visualized Experiments)*, (187):e64442, September 2022. ISSN 1940-087X. doi: 10.3791/64442. URL <https://www.jove.com/fr/v/64442/through-dog-s-eyes-fmri-decoding-naturalistic-videos-from-dog>.
- Ana Luísa Pinho, Alexis Amadon, Torsten Ruest, Murielle Fabre, Elvis Dohmatob, Isabelle Denghien, Chantal Ginisty, Séverine Becuwe-Desmidt, Séverine Roger, Laurence Laurier, Véronique Joly-Testault, Gaëlle Médiouni-Cloarec, Christine Doublé, Bernadette Martins, Philippe Pinel, Evelyn Eger, Gaël Varoquaux, Christophe Pallier, Stanislas Dehaene, Lucie Hertz-Pannier, and Bertrand Thirion. Individual Brain Charting, a high-resolution fMRI dataset for cognitive mapping. *Scientific Data*, 5(1):180105, June 2018. ISSN 2052-4463. doi: 10.1038/sdata.2018.105. URL <https://www.nature.com/articles/sdata2018105>. Number: 1 Publisher: Nature Publishing Group.
- Alec Radford, Jong Wook Kim, Chris Hallacy, Aditya Ramesh, Gabriel Goh, Sandhini Agarwal, Girish Sastry, Amanda Askell, Pamela Mishkin, Jack Clark, Gretchen Krueger, and Ilya Sutskever. Learning Transferable Visual Models From Natural Language Supervision, February 2021. URL <http://arxiv.org/abs/2103.00020>. arXiv:2103.00020 [cs].
- Hugo Richard, Luigi Gresele, Aapo Hyvärinen, Bertrand Thirion, Alexandre Gramfort, and Pierre Ablin. Modeling Shared Responses in Neuroimaging Studies through MultiView ICA, December 2020. URL <http://arxiv.org/abs/2006.06635>. arXiv:2006.06635 [cs, stat].
- Emma C. Robinson, Saad Jbabdi, Matthew F. Glasser, Jesper Andersson, Gregory C. Burgess, Michael P. Harms, Stephen M. Smith, David C. Van Essen, and Mark Jenkinson. MSM: a new flexible framework for Multimodal Surface Matching. *NeuroImage*, 100:414–426, October 2014. ISSN 1095-9572. doi: 10.1016/j.neuroimage.2014.05.069.

- Paul S. Scotti, Atmadeep Banerjee, Jimmie Goode, Stepan Shabalin, Alex Nguyen, Ethan Cohen, Aidan J. Dempster, Nathalie Verlinde, Elad Yundler, David Weisberg, Kenneth A. Norman, and Tanishq Mathew Abraham. Reconstructing the Mind’s Eye: fMRI-to-Image with Contrastive Learning and Diffusion Priors, May 2023. URL <http://arxiv.org/abs/2305.18274>. arXiv:2305.18274 [cs, q-bio].
- Thibault Séjourné, François-Xavier Vialard, and Gabriel Peyré. The Unbalanced Gromov Wasserstein Distance: Conic Formulation and Relaxation. *arXiv:2009.04266 [math, stat]*, June 2021. URL <http://arxiv.org/abs/2009.04266>. arXiv: 2009.04266.
- Yu Takagi and Shinji Nishimoto. High-resolution image reconstruction with latent diffusion models from human brain activity, March 2023. URL <https://www.biorxiv.org/content/10.1101/2022.11.18.517004v3>. Pages: 2022.11.18.517004 Section: New Results.
- Jerry Tang, Amanda LeBel, Shailee Jain, and Alexander G. Huth. Semantic reconstruction of continuous language from non-invasive brain recordings. *Nature Neuroscience*, 26(5):858–866, May 2023. ISSN 1546-1726. doi: 10.1038/s41593-023-01304-9. URL <https://www.nature.com/articles/s41593-023-01304-9>. Number: 5 Publisher: Nature Publishing Group.
- Armin Thomas, Christopher Ré, and Russell Poldrack. Self-Supervised Learning of Brain Dynamics from Broad Neuroimaging Data. *Advances in Neural Information Processing Systems*, 35:21255–21269, December 2022. URL https://proceedings.neurips.cc/paper_files/paper/2022/hash/8600a9df1a087a9a66900cc8c948c3f0-Abstract-Conference.html.
- Alexis Thual, Quang Huy Tran, Tatiana Zemskova, Nicolas Courty, Rémi Flamary, Stanislas Dehaene, and Bertrand Thirion. Aligning individual brains with fused unbalanced Gromov Wasserstein. *Advances in Neural Information Processing Systems*, 35:21792–21804, December 2022. URL https://proceedings.neurips.cc/paper_files/paper/2022/hash/8906cac4ca58dcaf17e97a0486ad57ca-Abstract-Conference.html.
- Chong Wang, Hongmei Yan, Wei Huang, Jiyi Li, Yuting Wang, Yun-Shuang Fan, Wei Sheng, Tao Liu, Rong Li, and Huafu Chen. Reconstructing rapid natural vision with fMRI-conditional video generative adversarial network. *Cerebral Cortex*, 32(20):4502–4511, October 2022. ISSN 1047-3211. doi: 10.1093/cercor/bhab498. URL <https://doi.org/10.1093/cercor/bhab498>.
- Haiguang Wen, Junxing Shi, Yizhen Zhang, Kun-Han Lu, Jiayue Cao, and Zhongming Liu. Data for Neural Encoding and Decoding with Deep Learning for Dynamic Natural Vision Tests, September 2017. URL <https://purr.purdue.edu/publications/2809/1>.
- Haiguang Wen, Junxing Shi, Yizhen Zhang, Kun-Han Lu, Jiayue Cao, and Zhongming Liu. Neural Encoding and Decoding with Deep Learning for Dynamic Natural Vision. *Cerebral Cortex (New York, N.Y.: 1991)*, 28(12):4136–4160, December 2018. ISSN 1460-2199. doi: 10.1093/cercor/bhx268.

A APPENDIX

A.1 DATA PRE-PROCESSING

We strive to minimally preprocess acquired BOLD signal. To this end, we detrend acquired BOLD signal (i.e. we remove cosine drifts) and finally standardize voxels' timecourses for each run, as shown in Figure S1.

Moreover, when decoding the latent representation of a given image, we use brain volumes which have been acquired after the image's onset. Figure S2 illustrates this idea, and introduces the concepts of *window size* (i.e. the number of brain volumes we use) and *lag* (i.e. the time difference between the onset of the image to be decoded and the first brain volume used to decode it). Values for both of these hyper-parameters were cross-validated. We report these results in Figure S3.

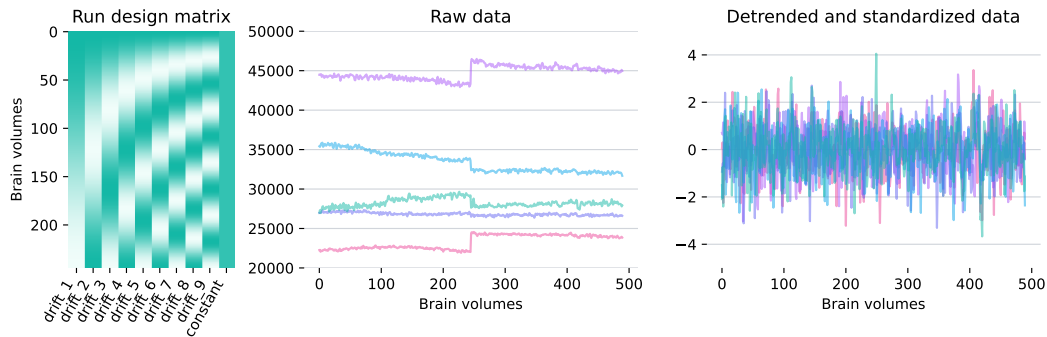


Figure S1: **Pre-processing of the Wen 2017 dataset** For each subject and each run, in each vertex, we regress out parts of the signal which can be linearly explained by the design matrix represented on the left, which models cosine drifts of the BOLD signal. The two graphs to the right show time-courses in 5 vertices across 2 different runs before (left) and after (right) they have been pre-processed.

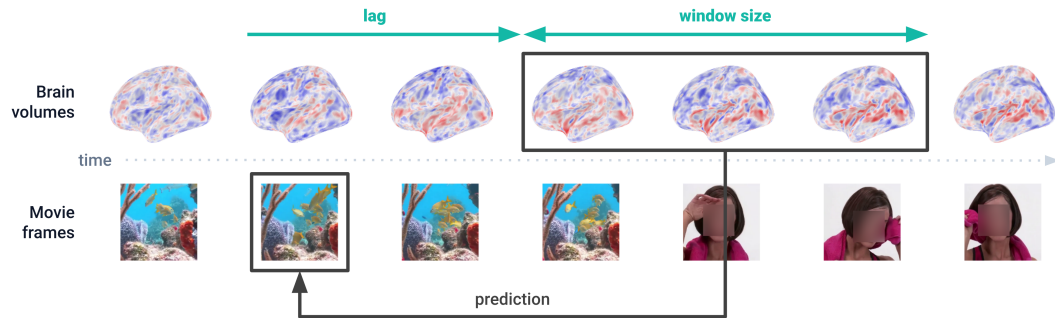


Figure S2: **Lag and window size** In order to decode a movie frame which was seen at time t , one can use brain volumes which were acquired further in time. This delay is referred to as the *lag*. Moreover, one can use several brain volumes to decode a given movie frame. The number of brain volumes used is called the *window size*. Images featuring human faces were blurred.

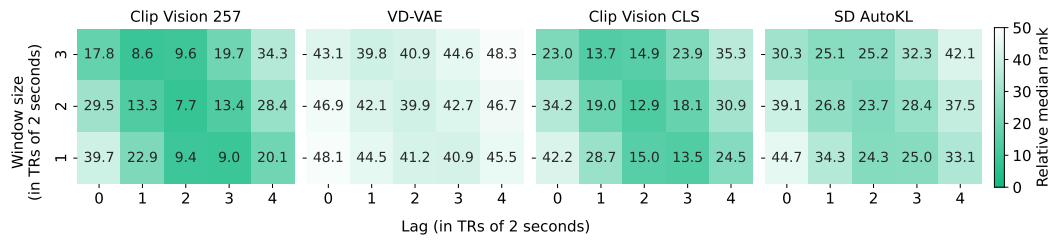


Figure S3: **Relative median rank ↓ of predicted latents averaged across subjects for various time lags and window sizes**

A.2 RETRIEVING IMAGES USING PREDICTED LATENT REPRESENTATIONS

Predicted latent representations can be compared to that of images in a retrieval set. In Figure S4, for each image shown to the subject during the test phase, we print the five images from the retrieval set whose latent representation is the closest to predicted latents. We see that semantics are often preserved.

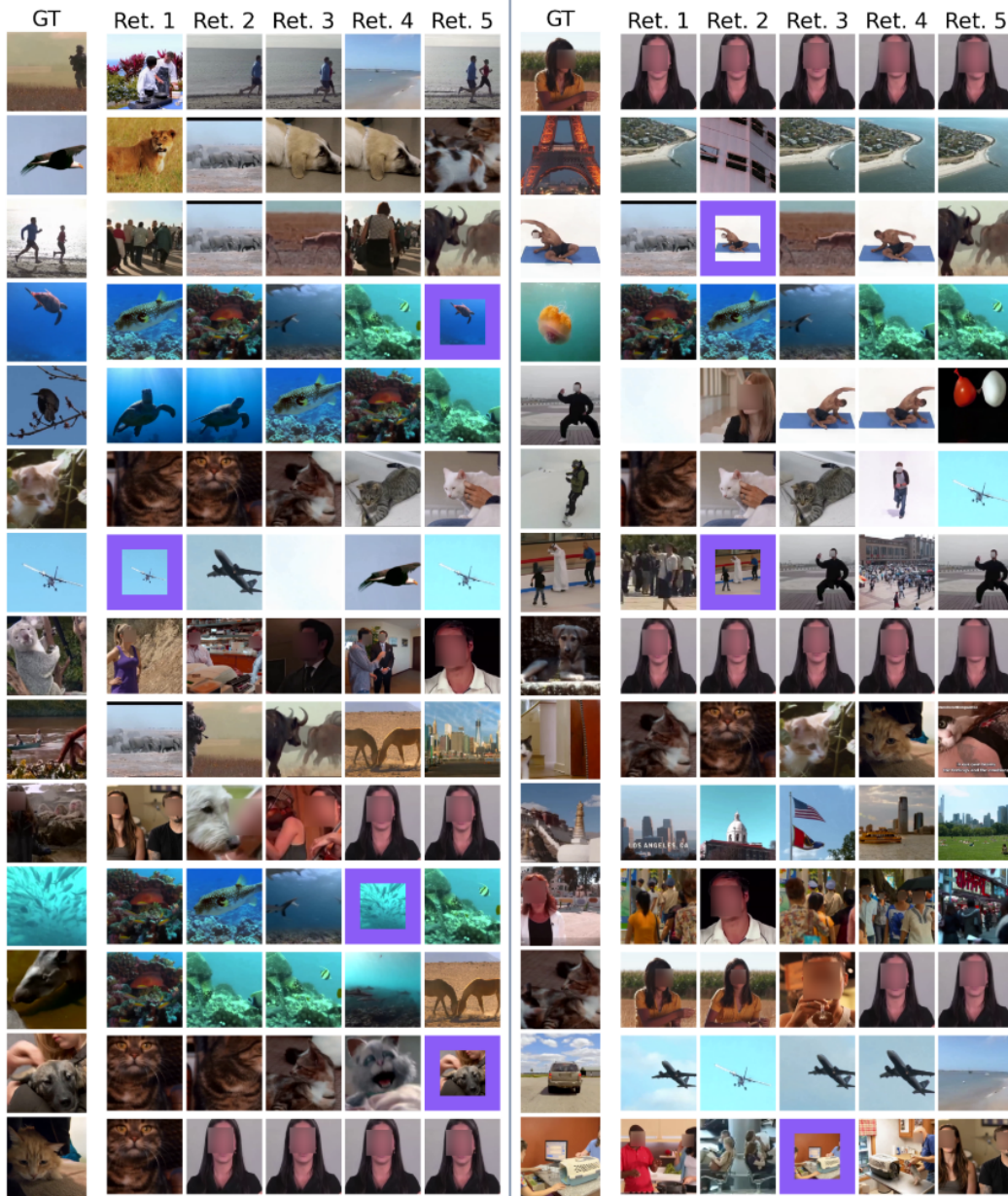


Figure S4: **Image retrievals using predicted latent representations of CLIP 257×768 latents**
 We use a model fitted on Subject 2 (S2) and predict the latent representation of unseen videos (test set). Ground truth (GT) images featured within the first 5 retrieved (Ret.) images are indicated with a bold purple border. In a given row, images which appear similar across columns are actually different frames of the same video clip. Images featuring human faces were blurred.

A.3 RESULTS FOR EVERY COMBINATION OF REFERENCE SUBJECT AND LEFT-OUT SUBJECT

Figure S5 is a copy of Figure 3 from the main pages of this paper. It illustrates the main effects reported in our study, namely that (1) functional alignment yields better performance than anatomical alignment when transferring a semantic decoder to left-out individuals, (2) it is possible to train such decoders on multiple subjects and (3) this last setup works best when subjects are aligned.

Figure S5 only shows these results when subject 2 of the Wen 2017 dataset is used as the reference subject. Therefore, we add Figures S6 and S7, which illustrate that all results hold regardless of what subject of the cohort is used as reference or left-out subject.

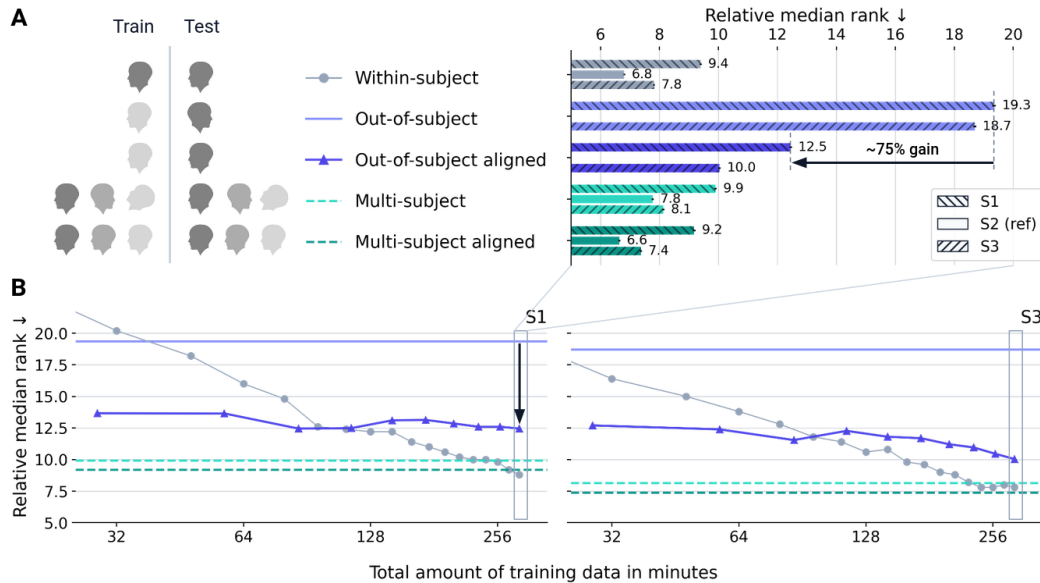


Figure S5: Effects of functional alignment on multi-subject and out-of-subject setups using subject 2 as the reference subject We report relative median rank \downarrow in all setups described in section 2.3 for CLIP 257×768 . In all *aligned* cases, S1 and S3 were aligned onto S2. In all *out-of-subject* cases, we test S1 and S3 onto a decoder trained on S2. In all *multi-subject* cases, the decoder was trained on all data from all 3 subjects. **A**. In this panel, all models (alignment and decoding) were trained on all available training data. Results for other latent types are available in Figure S8. **B**. In left-out S1 and S3, decoding performance is much better when using functional alignment to S2 (solid dark purple) than when using anatomical alignment only (solid pale purple). Performance increases slightly as the amount of data used to align subjects grows, but does not always reach levels which can be achieved with a single-subject model fitted in left-out subjects (solid pale gray dots) when a lot of training data is available. Training a model on multiple subjects yields good performance in all 3 subjects (dashed pale teal) which can be further improved by using functional alignment (dashed dark teal). Results for other latent types are available in Figure S9.

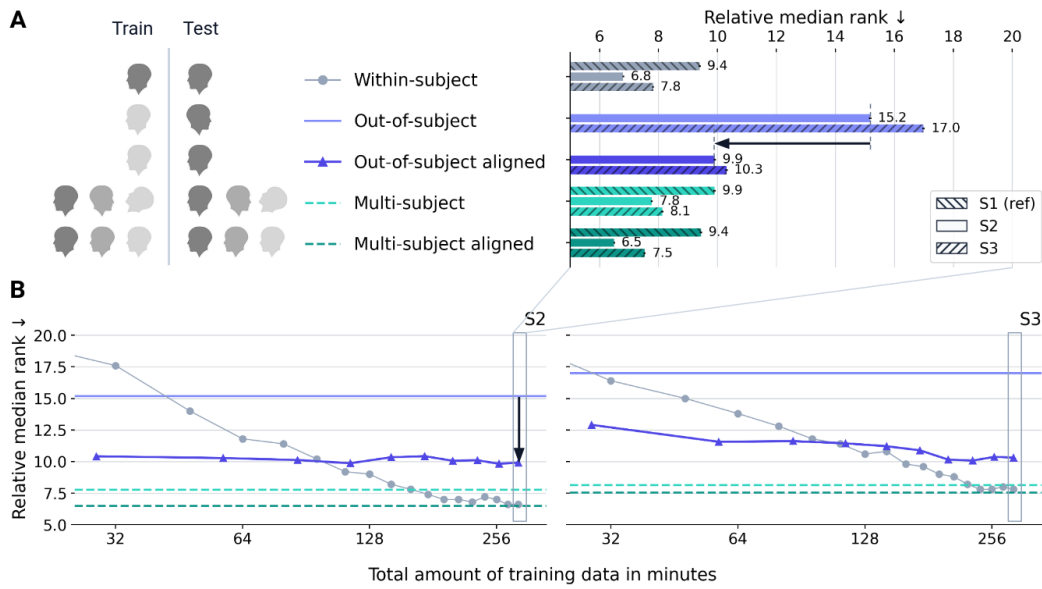


Figure S6: Effects of functional alignment on multi-subject and out-of-subject setups using subject 1 as the reference subject

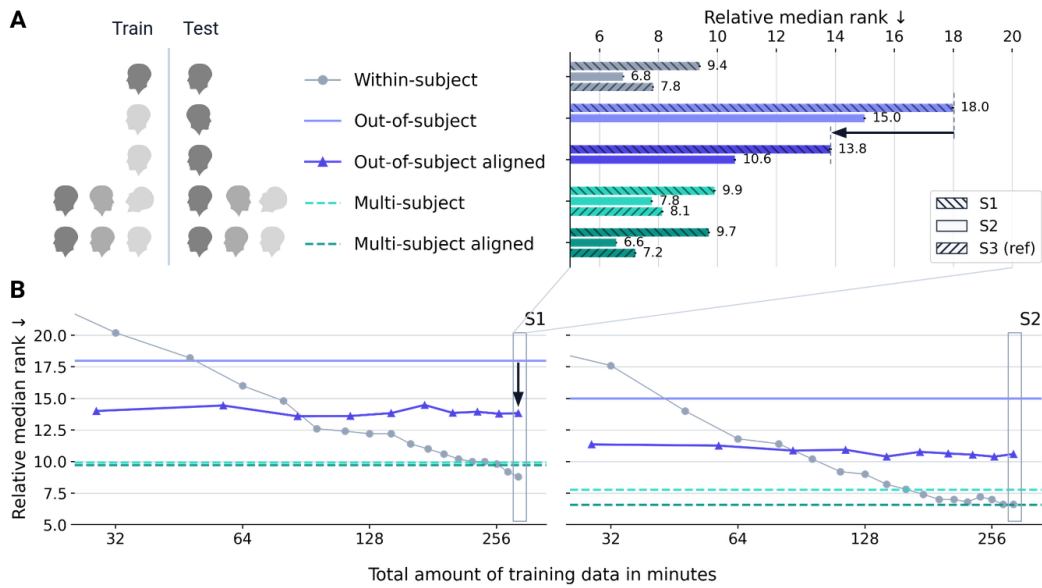


Figure S7: Effects of functional alignment on multi-subject and out-of-subject setups using subject 3 as the reference subject

A.4 REPLICATION ON THE NATURAL SCENES DATASET

We replicate our main experiment using data from the Natural Scenes Dataset (Allen et al., 2022). This dataset comprises 8 subjects who each see 10 000 images 3 times, thus leading to a total of 30 000 trials per subject. For each subject, this data is acquired in 40 sessions of 60 minutes each. For each subject, there is a total of 1 000 images which are shared with other individuals - i.e. other individuals will see them too - and 9 000 which are exclusive - i.e. other individuals will not see them. We sub-selected all subjects who had completed all 30 000 trials, namely subjects 1, 2, 5, and 7. For each selected subject, we split their 30 000 trials in two sets: all exclusive images are grouped in the *decoding set* and all shared images are grouped in the *alignment set*. We further split the decoding set into disjoint sets of images for training and testing individual decoders, whose performance is reported in Table S1. Alignments sets are used to compute functional alignments between individuals. Besides, we used pre-computed beta coefficients computed with GLM denoise on *fsaverage7* (Fischl, 2012) and openly available online. We down-sampled this data to *fsaverage5* - which simply amounts to keeping only the first 10 242 array elements in each hemisphere.

Eventually, we show that decoders tested on left-out individuals work consistently and significantly better when left-out subjects are functionally aligned rather than simply anatomically aligned to the reference subject, as reported in Table S2.

Table S1: **Within-subject metrics for all NSD subjects and all latent types on the test set** Reported metrics are relative median rank \downarrow (MR) of retrieval on a set of 500 samples, top-5 accuracy $\% \uparrow$ (Acc) of retrieval on a set of 500 samples. Chance level is at 50.0 and 1.0 for these metrics respectively. These results were averaged across 50 retrieval sets, hence results are reported with a standard error of the mean (SEM) smaller than 0.01.

	CLIP 257 \times 768		VD-VAE		CLIP CLS		AutoKL	
	MR	Acc	MR	Acc	MR	Acc	MR	Acc
S1	3.6	26.6	23.0	4.6	4.6	19.1	30.5	1.8
S2	6.0	17.6	22.1	4.4	6.9	13.8	33.6	1.5
S5	4.6	19.9	26.0	3.7	4.3	19.7	31.5	2.5
S7	4.0	24.4	23.4	5.4	5.5	18.5	24.5	4.3

Table S2: **Across-subject metrics for all NSD subjects and all latent types on the test set** We report the decoding performance of decoders trained on a reference subject and tested on a left-out subject who was anatomically aligned (A) or functionally aligned (A+F). The reported metric is the relative median rank \downarrow (MR) of retrieval on a set of 500 samples. These results were averaged across 50 retrieval sets, hence results are reported with a standard error of the mean (SEM) smaller than 0.01. One sees that functionally aligned data is always better decoded than anatomically aligned data.

Reference	Left-out	CLIP 257 \times 768		VD-VAE		CLIP CLS		AutoKL	
		A	A+F	A	A+F	A	A+F	A	A+F
S1	S2	20.9	10.7	35.2	24.5	28.3	13.4	42.5	37.1
	S5	32.2	13.6	43.1	32.0	33.4	12.5	43.9	37.7
	S7	33.5	14.7	40.8	30.7	36.1	17.1	45.0	37.0
S2	S1	18.3	10.4	37.0	30.4	24.4	14.4	35.9	37.1
	S5	29.3	12.0	40.3	34.1	30.8	11.2	42.4	39.6
	S7	27.9	14.6	40.2	32.8	32.1	17.9	41.8	38.9
S5	S1	29.2	13.0	43.4	34.4	33.8	14.4	37.8	33.8
	S2	26.2	9.8	40.1	30.1	31.4	11.2	36.0	36.2
	S7	29.8	14.1	41.7	32.0	34.4	17.3	40.0	34.9
S7	S1	27.7	7.7	43.1	30.1	32.3	11.5	40.6	26.5
	S2	23.4	8.6	38.9	26.4	28.6	13.2	37.8	29.1
	S5	27.5	8.8	41.6	31.2	30.4	9.8	43.4	30.9

A.5 RESULTS FOR EVERY TYPE OF LATENT REPRESENTATION

Results of supplementary section A.4 show that our effects of interest hold for CLIP 257×768 regardless of the combination of reference / left-out subjects. We replicate these experiments using 3 additional types of latent representations, namely VD-VAE, CLIP CLS and AutoKL and report results in Figures S8, S9 and S10. These figures show that all observed effects are present regardless of the chosen latent representation.

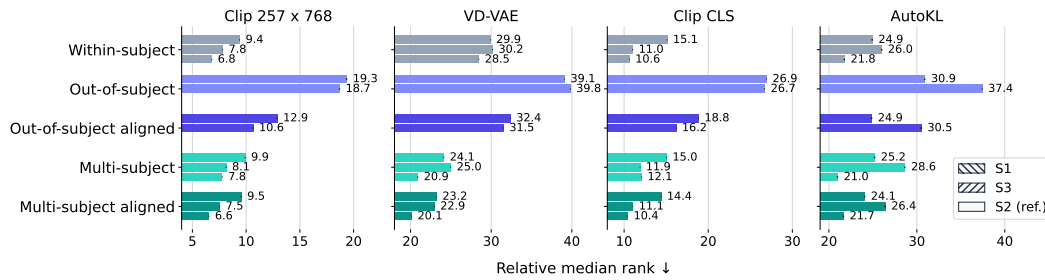


Figure S8: **Effects of alignment** For any type of latent representation, out-of-subject decoding performance, measured through relative median rank ↓, greatly improves when subjects are functionally aligned. Training decoders on multiple subjects also works better when subjects are aligned. These results were averaged across 50 retrieval sets ; all these metrics are reported with a standard error of the mean (SEM) smaller than 0.01.

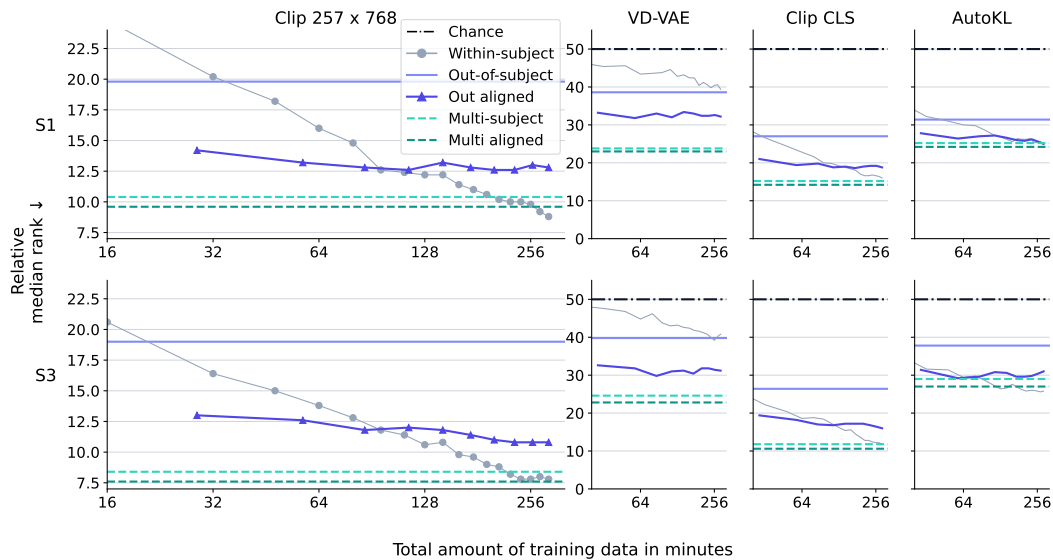


Figure S9: **Performance increases slightly with more alignment data** For any type of latent representation, out-of-subject decoding performance greatly increases with functional alignment even in low data regimes. In high data regimes, out-of-subject decoding does not work as well as fitting single-subject or multi-subject models.

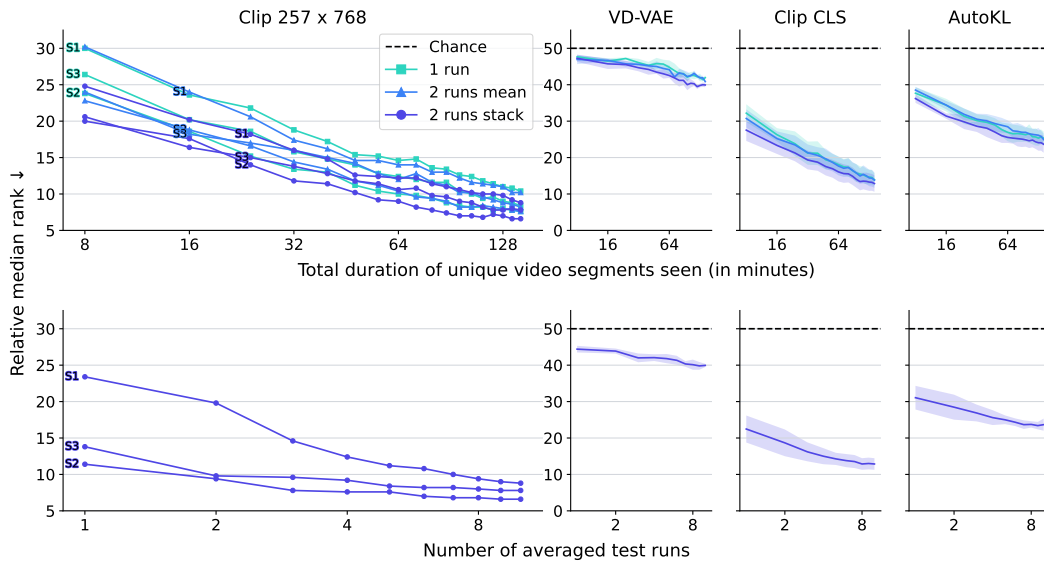


Figure S10: **Scaling studies for all latents** For any type of latent representation, decoding performance increases linearly with exponentially more data. It also seems that, when acquiring data at 3T or more, not repeating stimuli yields the best results. At test time, although repeating stimuli allows to get better metrics, retrieval performance with only one repetition is already reasonable in 2 out of 3 subjects of the Wen 2017 dataset.

S1	S2	S3	S4	S5	S6	S7	S8	S9	S10	S11	S12	S13	S14	S15	S16	S17	S18	S19	S20	S21	S22	S23	S24	S25	S26	S27	S28	S29	S30	S31	S32	S33	S34	S35	S36	S37	S38	S39	S40	S41	S42	S43	S44	S45	S46	S47	S48	S49	S50	S51	S52	S53	S54	S55	S56	S57	S58	S59	S60	S61	S62	S63	S64	S65	S66	S67	S68	S69	S70	S71	S72	S73	S74	S75	S76	S77	S78	S79	S80	S81	S82	S83	S84	S85	S86	S87	S88	S89	S90	S91	S92	S93	S94	S95	S96	S97	S98	S99	S100	No data	
																																																																																																				0	1
S1	S2	S3	S4	S5	S6	S7	S8	S9	S10	S11	S12	S13	S14	S15	S16	S17	S18	S19	S20	S21	S22	S23	S24	S25	S26	S27	S28	S29	S30	S31	S32	S33	S34	S35	S36	S37	S38	S39	S40	S41	S42	S43	S44	S45	S46	S47	S48	S49	S50	S51	S52	S53	S54	S55	S56	S57	S58	S59	S60	S61	S62	S63	S64	S65	S66	S67	S68	S69	S70	S71	S72	S73	S74	S75	S76	S77	S78	S79	S80	S81	S82	S83	S84	S85	S86	S87	S88	S89	S90	S91	S92	S93	S94	S95	S96	S97	S98	S99	S100	0	1

Figure S12: Relative median rank ↓ for VD-VAE latents in single- and multi-subject training sets, with and without alignment, tested on within- and across-subjects setups with and without alignment. These results were averaged across 50 retrieval sets ; all these metrics are reported with a standard error of the mean (SEM) smaller than 0.01.

